Rapid Communications

Approaching three-dimensional quantum Hall effect in bulk $HfTe_5$

Peng Wang,[1,2,*] Yafei Ren,[1,*] Fangdong Tang,[2,3] Peipei Wang,[2] Tao Hou,[1]
Hualing Zeng,[1,†] Liyuan Zhang,[2,‡] and Zhenhua Qiao[1,§]

[1]*International Center for Quantum Design of Functional Materials, Hefei National Laboratory for Physical Sciences at the Microscale, Synergetic Innovation Centre of Quantum Information and Quantum Physics, CAS Key Laboratory of Strongly Coupled Quantum Matter Physics, and Department of Physics, University of Science and Technology of China, Hefei 230026, China*

[2]*Department of Physics, Southern University of Science and Technology, and Shenzhen Institute for Quantum Science and Engineering, Shenzhen 518055, China*

[3]*Solid State Nanophysics, Max Plank Institute for Solid State Research, Stuttgart 70569, Germany*

(Received 5 January 2020; revised manuscript received 6 March 2020; accepted 9 March 2020; published 6 April 2020)

We report the electronic transport features of $HfTe_5$ under external magnetic field. We observe a series of plateaus in Hall resistance ρ_{xy} as magnetic field increases until it reaches the quantum limit at 1–2 Tesla. At the plateau regions, the longitudinal resistance ρ_{xx} exhibits local minima. Although ρ_{xx} is still nonzero, its value becomes much smaller than ρ_{xy} at the last few plateaus. By mapping the Fermi surface via measuring the Shubonikov–de Haas oscillation, we find that the strength of Hall plateau is proportional to the Fermi wavelength, suggesting that its formation may be attributed to the gap opening from the interaction driven Fermi surface instability. By comparing the bulk band structures of $ZrTe_5$ and $HfTe_5$, we find that there exists an extra pocket near the Fermi level of $HfTe_5$, which may lead to the finite but nonzero longitudinal conductance.

DOI: 10.1103/PhysRevB.101.161201

Introduction. The discovery of quantum Hall effect in two-dimensional (2D) electronic systems inspired the topological classifications of electronic systems [1,2]. By stacking 2D quantum Hall effects with interlayer coupling much weaker than the Landau level spacing, quasi-2D quantum Hall effects have been experimentally observed [3–7], due to the similar physical origin of the 2D counterpart. Recently, in a real three-dimensional (3D) electronic gas system where the interlayer coupling is much stronger than the Landau level spacing, 3D quantum Hall effect has been observed in $ZrTe_5$ [8]. Two benchmarks of the quantum Hall effect (QHE) are the quantized Hall resistance plateaus and vanishing longitudinal resistance [9]. The quantization originates from the presence of an energy gap, which appears once the Landau levels are formed under strong magnetic field [10]. By stacking layers of 2D QHE into a superlattice, the signatures of QHE can also be observed in bulk systems when the interlayer coupling becomes smaller than the Landau level spacings [11]. Such bulk QHE is regarded as quasi-2D as its nature is still closely related to the 2D case [12]. Recently, the evidence of genuine 3D QHE has been experimentally reported by electronic transport measurements in bulk $ZrTe_5$ materials under magnetic field [8] after being proposed theoretically over 30 years ago by Halperin [13]. In contrast to the quasi-2D case, the single-particle electronic bands under the magnetic field are gapless since the interlayer coupling is much larger than the Landau level spacing. An energy gap near the Fermi energy is evidenced by transport measurements originating from the formation of charge density wave driven by Coulomb interaction [8,14].

Comparing to 2D QHE that is universal and can be realized in a large number of 2D electronic systems, the material systems hosting 3D QHE are extremely limited. In this Rapid Communication, we report our experimental findings suggesting the approaching of 3D QHE in bulk $HfTe_5$ systems. We first demonstrate the 3D nature of the Fermi surface via Shubnikov–de Haas oscillations of longitudinal resistances by changing the orientation. We then measure the Hall and longitudinal resistances by increasing the magnetic field to the quantum limit where Landau levels are formed. We find quasiplateaus in Hall resistance and corresponding dips of longitudinal resistance, which together indicate the possible presence of 3D QHE. We show that the magnitude of the last Hall resistivity plateau ρ_{xy} is proportional to the Fermi wavelength $\lambda_{F,Z}$ along the z direction, i.e., $\rho_{xy} = \frac{h}{e^2}\frac{\lambda_{F,Z}}{2}$, where h is the Planck's constant and e is an elementary charge, following the same rules as those findings in $ZrTe_5$ [8]. These qualitatively similar results in $HfTe_5$ as those in $ZrTe_5$ suggest the same physical origin underlying both cases, i.e., a 3D QHE induced by Fermi surface instability driven by Coulomb interaction. Nevertheless, one can see that though the longitudinal resistance is much smaller than the corresponding Hall resistance, it does not completely decrease to be vanishing at the last plateau region. We attribute the possible physical origin to the emergence of a multiband around the Fermi surface of $HfTe_5$.

$HfTe_5$ is an orthorhombic layered structure composed of one-dimensional atomic chains along the a direction and

*These authors contributed equally to this work.
†hlzeng@ustc.edu.cn
‡zhangly@sustech.edu.cn
§qiao@ustc.edu.cn

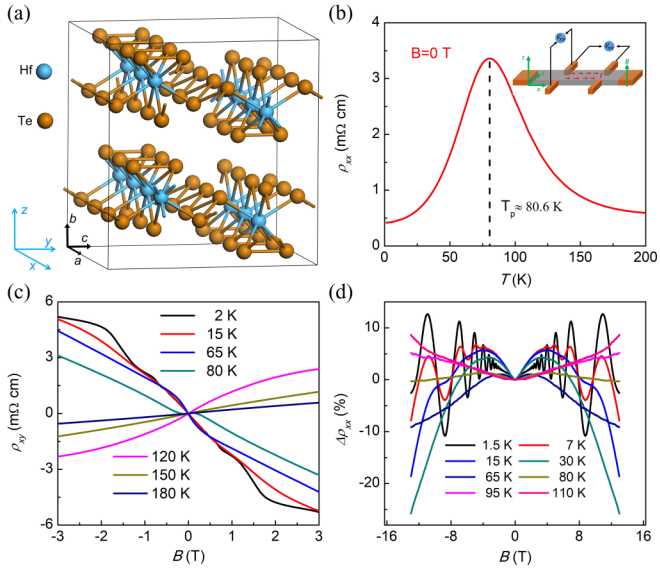

FIG. 1. Structure and three-dimensional nature of $HfTe_5$. (a) Crystal structure of $HfTe_5$. (b) Temperature dependence of resistivity of bulk $HfTe_5$. There is a peak at about 80.6 K labeled by a dashed line. The inset illustrates the setup of our transport measurement. (c) Magnetic field dependence of Hall resistivity at different tempratures. When it is higher than 80 K, the sign changes, which means the main carrier transits from electron to hole. (d) The parallel magnetic field dependence of resistivity ($\Delta\rho_{xx} = \frac{\rho_{xx}(B)-\rho_{xx}(0)}{\rho_{xx}(0)}$) at different temperatures.

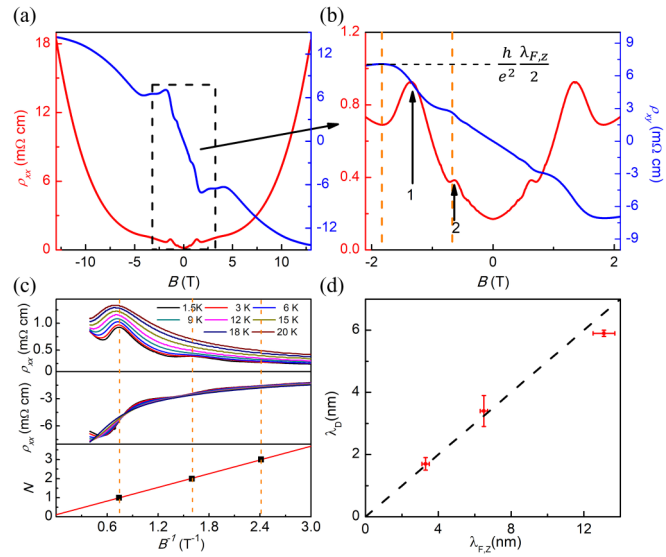

FIG. 2. Signatures and analysis of 3D QHE. (a) Out-of-plane perpendicular magnetic field dependence of longitudinal (red) and Hall (blue) resistivity from 13 to −13 T at 1.5 K. (b) The zoom-in of the dashed frame in (a). We can find that every Hall plateau corresponds to the dip of a ρ_{xx} marked by yellow dashed lines. The black dashed line marks the last Hall plateau whose resistivity equals to $\frac{h}{e^2}\frac{\lambda_{F,Z}}{2}$. The arrows and numbers refer to the Landau factor extracted by (c). (c) The ρ_{xx} and ρ_{xy} versus $1/B$ at different temperatures and the Landau fan diagram. The yellow dashed lines mark the position of the peak of ρ_{xx}. (d) Period λ_D versus z-direction Fermi wavelength $\lambda_{F,Z}$, the ratio is almost about 0.5, which is fitted by a dashed line.

the layer stacking along the b direction as illustrated in Fig. 1(a) [15], where the a, b, and c directions are set to be along the x, z, and y axes. This material is topologically the same as $ZrTe_5$, which is considered as either a strong topological insulator or a weak topological insulator [16–21], depending on the detailed material parameters. We measure the longitudinal and Hall resistances of bulk $HfTe_5$ systems with thicknesses of tens of micrometers at different temperatures ranging from 1.5 to 200 K by using the six-electrode Hall-bar geometry as schematically plotted in the inset of Fig. 1(b).

The longitudinal resistivity ρ_{xx} of $HfTe_5$ exhibits an anomalous dependence on temperature as displayed in Fig. 1(b), where ρ_{xx} first increases and then decreases as temperature increases, with a peak that appears at T_p of 80.6 K. By measuring the Hall effect at different temperatures as displayed in Fig. 1(c), we find that the carrier type is electronlike when $T < T_p$, whereas it becomes holelike when $T > T_p$. This phenomenon is consistent with the angle-resolved photoemission spectroscopy (ARPES) results, i.e., the Fermi energy transitions from valence band to conduction band when temperature decreases [22].

3D Fermi surface. After characterizing the samples in our experiments, we move to measure the Hall effect. We first try to detect the 3D nature of the electronic structure, i.e., a closed Fermi surface. By measuring the dependence of longitudinal resistivity ρ_{xx} as a function of magnetic field, we find the presence of Shubnikov–de Haas oscillation for the magnetic field along different orientations (see Sec. I of the Supplemental Material for the detailed results [23]). In particular, as displayed in Fig. 1(d), we plot the longitudinal resistance as a function of the parallel magnetic field with the electric current. We show that, at temperatures up to 7 K, the clear Shubnikov–de Haas oscillation still appears. This suggests that the electrons' motion in the x-z or the y-z plane is coherent and the Fermi surface is closed [8]. And we also find an obvious negative magnetoresistance which could be attributed to the chiral anomaly observed in many other materials [24–30].

3D QHE at 1.5 K. We then focus on the electronic transport properties at a low temperature of 1.5 K. From both the longitudinal and Hall resistances at low magnetic field, we extract the carrier densities and mobilities of our samples, which are respectively 10^{16}–10^{17} cm^{-3} and 100 000–146 000 cm^2 V^{-1} s^{-1} (see Sect. II of the Supplemental Material for the detailed fitting results). One can see that our samples exhibit very low carrier density and extremely high mobility. By applying the magnetic field along the z direction, we observe the plateaus of Hall resistance ρ_{xy} and oscillations of longitudinal resistance ρ_{xx} when the applied magnetic field increases, as displayed in Fig. 2(a). In the low-field region in Fig. 2(b), we observe a series of oscillations of ρ_{xx}. The Landau filling factor N can be extracted from the Landau fan diagram as displayed in Fig. 2(c), where the peak positions of ρ_{xx} are marked by integers, and the valleys are marked by half integers. We find that the quasiplateaus of

TABLE I. Relation between Fermi wavelength and period λ_D for three different samples. The detailed method to get $\lambda_{F,Z}$ is discussed in the Supplemental Material and λ_D is calculated by the last plateau according to the equation $\rho_{xy,n} = \frac{h}{e^2}\lambda_D$, $d = 0.725$ nm is the thickness of each atomic layer.

Sample	Sample No. 1	Sample No. 2	Sample No. 3
$\lambda_{F,Z}$ (nm)	6.5 ± 0.2	13.1 ± 0.6	3.3 ± 0.2
λ_D (nm)	3.4 ± 0.5	5.9 ± 0.1	1.7 ± 0.2
$\lambda_D/\lambda_{F,Z}$	0.52 ± 0.1	0.45 ± 0.03	0.52 ± 0.1
$\lambda_{F,Z}/d$	9 ± 0.2	18 ± 0.9	4.5 ± 0.3

ρ_{xy} correspond to the filling factors from $N = 2$ to $N = 1$ as labeled by numbers. Moreover, we find that at about $B = 1.8$ T the system reaches the extreme quantum limit, i.e., only the lowest Landau band being occupied. Qualitatively, our results are quite similar to that of 2D QHE, i.e., in the dip regimes of ρ_{xx}, ρ_{xy} exhibits plateaus. However, quantitatively, there are some differences.

The magnitude of the last Hall resistance plateau is about 0.7 Ω that is much smaller than 25.8 kΩ in 2D QHE, strongly suggesting that the Hall resistance plateau in our studies originates from the 3D bulk system but not from the 2D system. To better reflect the 3D nature of the Hall effect, we express the Hall resistivity to be $\rho_{xy} = \frac{h}{e^2}\lambda_D$ following Halperin's work [13], which indicates that the sample with a thickness of λ_D contributes to a quantized Hall conductance of $\frac{e^2}{h}$ at the $N = 1$ plateau. In this manner, we can assume the bulk system under magnetic field as a superstructure with many supercells and the thickness λ_D along the field direction. By comparing λ_D with the Fermi wavelength $\lambda_{F,Z}$ along the field direction, i.e., z direction, we find that the ratio of $\frac{\lambda_D}{\lambda_{F,Z}}$ is always about 1/2 for all three samples as displayed in Fig. 2(d) and Table I (see Sec. I of the Supplemental Material for details). Such a relation following the same rule as demonstrated in Ref. [8] suggests the presence of an energy gap at the Fermi energy due to the possible formation of charge density wave state [14,31,32]. Nevertheless, the nonzero longitudinal resistance preserves indicating that the gap might be smeared by disorder or there are other conducting electrons near the Fermi level contributing to finite conductance as discussed below.

To explore the possible underlying physical origin of nonzero ρ_{xx}, we first measure the dependence of the lowest $\rho_{xx}(B)$ at lower temperature as shown in Fig. S4 in the Supplemental Material. We find that the minimal magnitude of longitudinal resistance ρ_{xx} shows weak dependence on temperature and saturates as temperature decreases, which indicates that the lowest value of ρ_{xx} is not limited by the temperature. By further comparing the relative magnitude of $\rho_{\min}/\rho_{xx}(B = 0)$ for different samples with different mobilities, we notice that as mobility increases, $\rho_{\min}/\rho_{xx}(B = 0)$ shows the trend to decrease as shown in Fig. S5 of the Supplemental Material.

Comparing to the extremely large magnitudes of that in $ZrTe_5$ samples, i.e., 5×10^5 cm^2 V^{-1} s^{-1}, our best $HfTe_5$ sample exhibits mobility of about 2×10^5 cm^2 V^{-1} s^{-1}. Thus, one possible reason for the presence of finite $\rho_{\min}$ is that the mobilities of our $HfTe_5$ samples are yet not high enough. Alternatively, another possible reason lies in the difference between band structures of $HfTe_5$ and $ZrTe_5$. Both experimental and theoretical results indicate that the lattice constants of both materials would decrease as temperature decreases [33]. By employing lattice constants at low temperature, our calculations by WIEN2K suggest that the valley near the M point will become lower than that near the Γ point in $HfTe_5$, whereas in $ZrTe_5$, the valley near the Γ point is always the lowest one as displayed in Fig. 3 (see more details in Sec. VI of the Supplemental Material). Such kind of difference between $ZrTe_5$ and $HfTe_5$ leads to different carrier types that contribute to the longitudinal conductance. For the $ZrTe_5$ case, only the topological bands near the Γ point contribute to the electronic transport, while for the $HfTe_5$ case in this Rapid Communication, the electrons at the M valley may also be involved in the electronic transport, resulting in the nonzero longitudinal resistance when the band around Γ enters the extreme quantum limit region.

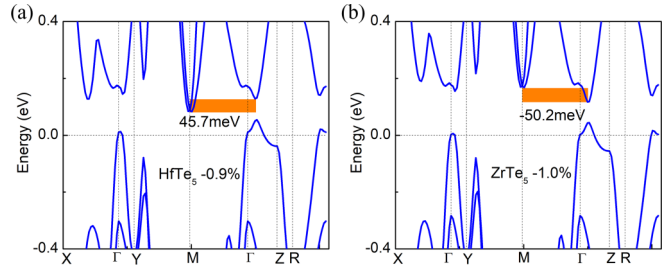

FIG. 3. The comparison of the band structure between $HfTe_5$ and $ZrTe_5$. (a) The calculated $HfTe_5$ band structure based on the experimental lattice constant at 10 K by WIEN2K. The −0.9% means that the volume of bulk $HfTe_5$ at 10 K is 0.9% smaller than 293 K. The energy difference between the Γ point and the M point is 45.7 meV, which is marked by the orange range. (b) $ZrTe_5$ band structure based on the experimental lattice constant at 10 K by WIEN2K whose volume is 1.0% smaller than 293 K. The energy difference between the Γ point and the M point is −50.2 meV.

Metal-insulator transition under high magnetic field. When we further increase the magnetic field to the extreme quantum limit, the longitudinal and Hall resistances stop oscillating as displayed in Fig. 2(a). The longitudinal resistance ρ_{xx} exhibits an unsaturated magnetoresistance, which can reach 10 000% of the zero-field resistance at the magnetic field of 13 T. Simultaneously, the Hall resistance ρ_{xy} keeps increasing to saturation in a nonlinear manner. By varying temperatures, we find that the oscillation of Hall resistance becomes smoother, whereas the turning point at the last resistance plateau is quite robust up to the temperature of about 12 K as displayed in Fig. 4(a). Moreover, we also find a metal-insulator transition at the extreme quantum limit as displayed in Fig. 4(b), which is characterized by the longitudinal resistance at a critical transition point of $B_C \approx 7.07$ T. We find that, at $B < B_C$, ρ_{xx} increases as temperature increases, which behaves like a metal; whereas at $B > B_C$, ρ_{xx} decreases as temperature increases, which behaves like an insulator. Near the phase transition point, ρ_{xx} is weakly dependent on

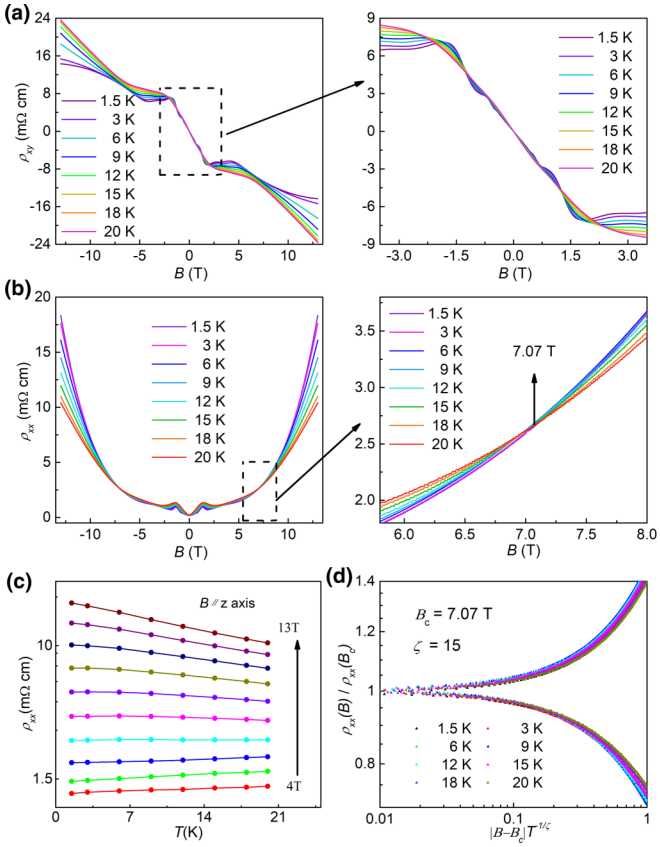

FIG. 4. High magnetic field dependence of longitudinal and Hall resistivity. (a) The magnetic field dependence of Hall resistivity ρ_{xy} at different temperatures T ranging from 1.5 to 20 K. (b) The magnetic field dependence of longitudinal resistivity ρ_{xx} at different temperatures T ranging from 1.5 to 20 K. On the right is the zoom-in image of the transition region near $B_C = 7.07$ T marked by a dashed box in the left figure. (c) The temperature dependence of longitudinal resistivity ρ_{xx} at different magnetic fields B ranging from 4 to 13 T. We can find the tendency of the curve is different at low field and high field. (d) The normalized resistance $\rho_{xx}/\rho_{xx}(B_C)$ as a function of the scaling variable $|B - B_C|T^{-1/\zeta}$ at different temperatures. The best fitting parameter is at $\zeta = 15$.

the temperature as displayed in Fig. 4(c). To further characterize the phase transition, we perform a scaling analysis of ρ_{xx} against the scaling variable $(B - B_C)T^{-1/\zeta}$ where ζ is the fitting parameter as displayed in Fig. 4(d). We find that $\zeta \cong 15$, which does not agree with the metal-insulator transition in 2D QHE either with or without spin degeneracy of Landau levels [34]. Moreover, by changing the temperature range, we find different values of ζ (see more details in Sec. IX of the Supplemental Materials). Thus, the phase transition cannot fit to the universality classes in 2D QHE and the nature of the insulating phase deserves further exploration in the future.

Summary. We report that bulk $HfTe_5$ (the cousin material of $ZrTe_5$) in the presence of a magnetic field can approach the 3D QHE with quantized Hall conductance and finite longitudinal resistance at the extreme quantum limit. By applying a magnetic field perpendicular to the atomic layers of bulk $HfTe_5$ and increasing it to the quantum limit, we observe Hall resistance plateaus and the corresponding longitudinal resistances show corresponding dips. After comparing the thickness of each supercell that contributes to a quantum Hall conductivity λ_D and the Fermi wavelength $\lambda_{F,Z}$, we find that $\frac{\lambda_D}{\lambda_{F,Z}}$ is about 1/2 for different samples, suggesting the presence of an energy gap. Nevertheless, the nonzero longitudinal resistance preserves which might be attributed to the presence of other conducting electrons near the Fermi level through our numerical calculation. Future experiments are still desired by using, for example, ARPES to demonstrate the electronic structure near the Fermi level [22,35].

Acknowledgments. The authors thank Prof. Hongming Weng for valuable discussions. This work was supported by National Key R&D Program (Grants No. 2017YFB0405703, No. 2017YFA0205004, and No. 2018YFA0306600), and the NNSFC (Grants No. 11974327, No. 11474265, No. 11674295, and No. 11674024), the Fundamental Research Funds for the Central Universities (Grants No. WK2030020032 and No. WK2340000082), and Anhui Initiative in Quantum Information Technologies. This work was partially carried out at the USTC Center for Micro and Nanoscale Research and Fabrication.

[1] K. V. Klitzing, G. Dorda, and M. Pepper, Phys. Rev. Lett. **45**, 494 (1980).
[2] D. C. Tsui, H. L. Stormer, and A. C. Gossard, Phys. Rev. Lett. **48**, 1559 (1982).
[3] S. T. Hannahs, J. S. Brooks, W. Kang, L. Y. Chiang, and P. M. Chaikin, Phys. Rev. Lett. **63**, 1988 (1989).
[4] J. R. K. Cooper, W. Auban, P. Montambaux, G. D. Jérome, and K. Bechgaard, Phys. Rev. Lett. **63**, 1984 (1989).
[5] S. Hill, S. Uji, M. Takashita, C. Terakura, T. Terashima, H. Aoki, J. S. Brooks, Z. Fisk, and J. Sarrao, Phys. Rev. B **58**, 10778 (1998).
[6] H. Cao, J. Tian, I. Miotkowski, T. Shen, J. Hu, S. Qiao, and Y. P. Chen, Phys. Rev. Lett. **108**, 216803 (2012).
[7] H. Masuda, H. Sakai, M. Tokunaga, Y. Yamasaki, A. Miyake, J. Shiogai, S. Nakamura, S. Awaji, A. Tsukazaki, H. Nakao, Y. Murakami, T. H. Arima, Y. Tokura, and S. Ishiwata, Sci. Adv. **2**, e1501117 (2016).
[8] F. D. Tang, Y. F. Ren, P. P. Wang, R. D. Zhong, J. Schneeloch, S. Y. Yang, K. Yang, P. A. Lee, G. D. Gu, Z. H. Qiao, and L. Y. Zhang, Nature (London) **569**, 537 (2019).
[9] L. Sheng, D. N. Sheng, F. D. M. Haldane, and L. Balents, Phys. Rev. Lett. **99**, 196802 (2007).
[10] R. B. Laughlin, Phys. Rev. B **23**, 5632 (1981).
[11] H. L. Störmer, J. P. Eisenstein, A. C. Gossard, W. Wiegmann, and K. Baldwin, Phys. Rev. Lett. **56**, 85 (1986).
[12] M. Shayegan, T. Sajoto, M. Santos, and C. Silvestre, Appl. Phys. Lett. **53**, 791 (1988).

[13] B. I. Halperin, Jpn. J. Appl. Phys. **26**, 1913 (1987).
[14] A. Bardasis and S. D. Sarma, Phys. Rev. B **29**, 780 (1984).
[15] S. Furuseth, L. Brattas, and A. Kjekshus, Acta Chem. Scand. **27**, 2367 (1973).
[16] Z. Fan, Q. F. Liang, Y. B. Chen, S. H. Yao, and J. Zhou, Sci. Rep. **7**, 45667 (2017).
[17] P. Shahi, D. J. Singh, J. P. Sun, L. X. Zhao, G. F. Chen, Y. Y. Lv, J. Li, J. Q. Yan, D. G. Mandrus, and J. G. Cheng, Phys. Rev. X **8**, 021055 (2018).
[18] H. M. Weng, X. Dai, and Z. Fang, Phys. Rev. X **4**, 011002 (2014).
[19] S. Liu, M. X. Wang, C. Chen, X. Xu, J. Jiang, L. X. Yang, H. F. Yang, Y. Y. Lv, J. Zhou, Y. B. Chen, S. H. Yao, M. H. Lu, Y. F. Chen, C. Felser, B. H. Yan, Z. K. Liu, and Y. L. Chen, APL Mater. **6**, 121111 (2018).
[20] H. Wang, C.-K. Li, H. Liu, J. Yan, J. Wang, J. Liu, Z. Lin, Y. Li, Y. Wang, L. Li, D. Mandrus, X. C. Xie, J. Feng, and J. Wang, Phys. Rev. B **93**, 165127 (2016).
[21] M. W. Oh, B. S. Kim, S. D. Park, D. M. Wee, and H. W. Lee, Solid State Commun. **146**, 454 (2008).
[22] Y. Zhang, C. L. Wang, G. D. Liu, A. J. Liang, L. X. Zhao, J. W. Huang, Q. Gao, B. Shen, J. Liu, C. Hu, W. J. Zhao, G. F. Chen, X. W. Jia, L. Yu, L. Zhao, S. L. He, F. F. Zhang, S. J. Zhang, F. Yang, Z. M. Wang, Q. J. Peng, Z. Y. Xu, C. T. Chen, and X. J. Zhou, Sci. Bull. **62**, 950 (2017).
[23] See Supplemental Material at http://link.aps.org/supplemental/10.1103/PhysRevB.101.161201 for the raw data of Shubonikov–de Haas oscillations and the methods of calculating Fermi wavelength, for carrier density and mobility of $HfTe_5$, for calculation of band structures of $HfTe_5$ and $ZrTe_5$, and for scaling behavior of metal-insulator transition.
[24] J. Xiong, S. K. Kushwaha, T. Liang, J. W. Krizan, M. Hirschberger, W. Wang, R. J. Cava, and N. P. Ong, Science **350**, 413 (2015).
[25] X. C. Huang, L. X. Zhao, Y. J. Long, P. P. Wang, D. Chen, Z. H. Yang, H. Liang, M. Q. Xue, H. M. Weng, Z. Fang, X. Dai, and G. F. Chen,Phys. Rev. X **5**, 031023 (2015).
[26] X. Yang, Y. Li, Z. Wang, Y. Zhen, and Z. Xu, arXiv:1506.02283.
[27] Z. Wang, Y. Zheng, Z. Shen, Y. Lu, H. Fang, F. Sheng, Y. Zhou, X. Yang, Y. Li, C. Feng, and Z. A. Xu, Phys. Rev. B **93**, 121112 (2016).
[28] F. Arnold, C. Shekhar, S. C. Wu, Y. Sun, M. Schmidt, N. Kumar, A. G. Grushin, J. H. Bardarson, R. D. dos Reis, M. Naumann, M. Baenitz, H. Borrmann, M. Nicklas, E. Hassinger, C. Felser, and B. H. Yan, Nat. Commun. **7**, 11615 (2016).
[29] C. Z. Li, L. X. Wang, H. Liu, J. Wang, Z. M. Liao, and D. P. Yu, Nat. Commun. **6**, 10137 (2015).
[30] Q. Li, D. E. Kharzeev, C. Zhang, Y. Huang, I. Pletikosic, A. V. Fedorov, R.D. Zhong, J. A. Schneeloch, G. D. Gu, and T. Valla, Nat. Phys. **12**, 550 (2016).
[31] J. A. Wilson, F. J. Di Salvo, and S. Mahajan, Adv. Phys. **24**, 117 (1975).
[32] W. L. McMillan, Phys. Rev. B **14**, 1496 (1976).
[33] H. Fjellvag and A. Kjekshus, Solid State Commun. **60**, 91 (1986).
[34] T. Wang, K. P. Clark, G. F. Spencer, A. M. Mack, and W. P. Kirk, Phys. Rev. Lett. **72**, 709 (1994).
[35] Y. Zhang, C. L. Wang, L. Yu, G. D. Liu, A. J. Liang, J. W. Huang, S. M. Nie, X. Sun, Y. X. Zhang, B. Shen, J. Liu, H. M. Weng, L. X. Zhao, G. F. Chen, X. W. Jia, C. Hu, Y. Ding, W. J. Zhao, Q. Gao, C. Li, S. L. He, L. Zhao, F. F. Zhang, S. J. Zhang, F. Yang, Z. M. Wang, Q. J. Peng, X. Dai, Z. Fang, Z. Y. Xu, C. T. Chen, and X. J. Zhou, Nat. Commun. **8**, 15512 (2017).